Forbush Decreases and <2 Day GCR Flux Non-recurrent Variations Studied with LISA Pathfinder

Armano, M ; Audley, H ; Baird, J ; Benella, S ; Binetruy, P ; Born, M ; Bortoluzzi, D ; Castelli, E ; Cavalleri, A ; Cesarini, A ; Cruise, A M ; Danzmann, K ; Silva, M de Deus ; Diepholz, I ; Dixon, G ; Dolesi, R ; Fabi, M ; Ferraioli, L ; Ferroni, V ; Finetti, N ; Fitzsimons, E D ; Freschi, M ; Gesa, L ; Gibert, F ; Giardini, D ; Giusteri, R ; Grimani, C ; Grzymisch, J ; Harrison, I ; Heinzel, G ; Jetzer, Philippe ; et al

Abstract: Non-recurrent short-term variations of the galactic cosmic-ray (GCR) flux above 70 MeV n−1 were observed between 2016 February 18 and 2017 July 3 on board the European Space Agency LISA Pathfinder (LPF) mission orbiting around the Lagrange point L1 at 1.5 × 106 km from Earth. The energy dependence of three Forbush decreases is studied and reported here. A comparison of these observations with others carried out in space down to the energy of a few tens of MeV n−1 shows that the same GCR flux parameterization applies to events of different intensity during the main phase. FD observations in L1 with LPF and geomagnetic storm occurrence are also presented. Finally, the characteristics of GCR flux non-recurrent variations (peaks and depressions) of duration <2 days and their association with interplanetary structures are investigated. It is found that, most likely, plasma compression regions between subsequent corotating high-speed streams cause peaks, while heliospheric current sheet crossing causes the majority of the depressions.

DOI: https://doi.org/10.3847/1538-4357/ab0c99

The Astrophysical Journal, 874:167 (15pp), 2019 April 1 https://doi.org/10.3847/1538-4357/ab0c99

Forbush Decreases and <2 Day GCR Flux Non-recurrent Variations Studied with *LISA Pathfinder*

M. Armano[1], H. Audley[2], J. Baird[3], S. Benella[4,5], P. Binetruy[6,24], M. Born[2], D. Bortoluzzi[7], E. Castelli[8], A. Cavalleri[9], A. Cesarini[4,5], A. M. Cruise[10], K. Danzmann[2], M. de Deus Silva[1], I. Diepholz[2], G. Dixon[10], R. Dolesi[8], M. Fabi[4], L. Ferraioli[11], V. Ferroni[8], N. Finetti[5,12], E. D. Fitzsimons[13], M. Freschi[1], L. Gesa[14], F. Gibert[8], D. Giardini[11], R. Giusteri[8], C. Grimani[4,5], J. Grzymisch[15], I. Harrison[16], G. Heinzel[2], M. Hewitson[2], D. Hollington[3], D. Hoyland[10], M. Hueller[8], H. Inchauspé[6], O. Jennrich[15], P. Jetzer[17], N. Karnesis[2], B. Kaune[2], N. Korsakova[18], C. J. Killow[18], K. Kudela[19,25], M. Laurenza[5,20], J. A. Lobo[14,26], I. Lloro[14], L. Liu[8], J. P. López-Zaragoza[14], R. Maarschalkerweerd[16], D. Mance[11], N. Meshksar[11], V. Martín[14], L. Martin-Polo[1], J. Martino[6], F. Martin-Porqueras[1], I. Mateos[14], P. W. McNamara[15], J. Mendes[16], L. Mendes[1], M. Nofrarias[14], S. Paczkowski[2], M. Perreur-Lloyd[18], A. Petiteau[6], P. Pivato[8], E. Plagnol[6], J. Ramos-Castro[21], J. Reiche[2], D. I. Robertson[18], F. Rivas[14], G. Russano[8], J. Slutsky[22], C. F. Sopuerta[14], T. Sumner[3], D. Telloni[5,23], D. Texier[1], J. I. Thorpe[22], D. Vetrugno[8], M. Villani[4,5], S. Vitale[8], G. Wanner[2], H. Ward[18], P. Wass[3], W. J. Weber[8], L. Wissel[2], A. Wittchen[2], and P. Zweifel[11]

[1] European Space Astronomy Centre, European Space Agency Villanueva de la Cañada, E-28692 Madrid, Spain
[2] Albert-Einstein-Institut, Max-Planck-Institut für Gravitationsphysik und Leibniz Universität Hannover Callinstraße 38, D-30167 Hannover, Germany
[3] High Energy Physics Group, Physics Department, Imperial College London Blackett Laboratory, Prince Consort Road London, SW7 2BW, UK
[4] DISPEA, Università di Urbino "Carlo Bo," Via S. Chiara, 27 I-61029 Urbino, Italy; catia.grimani@uniurb.it
[5] INFN—Sezione di Firenze via G. Sansone, 1 I-150019, Sesto Fiorentino, Firenze, Italy
[6] APC, Univ Paris Diderot, CNRS/IN2P3, CEA/lrfu, Obs de Paris, Sorbonne Paris Cité, France
[7] Department of Industrial Engineering, University of Trento, via Sommarive 9, I-38123 Trento, and Trento Institute for Fundamental Physics and Application/INFN, Italy
[8] Dipartimento di Fisica, Università di Trento and Trento Institute for Fundamental Physics and Application INFN, I-38123 Povo, Trento, Italy
[9] Istituto di Fotonica e Nanotecnologie, CNR-Fondazione Bruno Kessler, I-38123 Povo, Trento, Italy
[10] The School of Physics and Astronomy, University of Birmingham Birmingham, UK
[11] Institut für Geophysik, ETH Zürich Sonneggstrasse 5 CH-8092, Zürich, Switzerland
[12] Dipartimento di Scienze Fisiche e Chimiche, Università degli Studi dell'Aquila, Via Vetoio, Coppito, I-67100 L'Aquila, Italy
[13] The UK Astronomy Technology Centre, Royal Observatory Edinburgh Blackford Hill, Edinburgh EH9 3HJ, UK
[14] Institut de Ciències de l'Espai (*ICE*, CSIC) Campus UAB, Carrer de Can Magrans s/n E-08193 Cerdanyola del Vallès Institut d'Estudis Espacial de Catalunya (IEEC) Edifici Nexus I, C/ Gran Capità 2-4, despatx 201 E-08034 Barcelona, Spain
[15] European Space Technology Centre, European Space Agency Keplerlaan 1 2200 AG Noordwijk, The Netherlands
[16] European Space Operations Centre European Space Agency, D-64293, Darmstadt, Germany
[17] Physik Institut, Universität Zürich Winterthurerstrasse 190 CH-8057 Zürich, Switzerland
[18] SUPA, Institute for Gravitational Research School of Physics and Astronomy, University of Glasgow Glasgow, G12 8QQ, UK
[19] Nuclear Physics Institute of the CAS, Řež, Czech Republic
[20] Istituto di Astrofisica e Planetologia Spaziali INAF, Roma, Italy
[21] Department d'Enginyeria Electrònica, Universitat Politècnica de Catalunya, E-08034 Barcelona, Spain
[22] Gravitational Astrophysics Lab, NASA Goddard Space Flight Center 8800 Greenbelt Road Greenbelt, MD 20771, USA
[23] Osservatorio Astrofisico di Torino, INAF Pino Torinese, Italy
Received 2018 September 24; revised 2019 February 20; accepted 2019 March 3; published 2019 April 4

Abstract

Non-recurrent short-term variations of the galactic cosmic-ray (GCR) flux above 70 MeV n^{-1} were observed between 2016 February 18 and 2017 July 3 on board the European Space Agency *LISA Pathfinder* (*LPF*) mission orbiting around the Lagrange point L1 at 1.5×10^6 km from Earth. The energy dependence of three Forbush decreases is studied and reported here. A comparison of these observations with others carried out in space down to the energy of a few tens of MeV n^{-1} shows that the same GCR flux parameterization applies to events of different intensity during the main phase. FD observations in L1 with *LPF* and geomagnetic storm occurrence are also presented. Finally, the characteristics of GCR flux non-recurrent variations (peaks and depressions) of duration <2 days and their association with interplanetary structures are investigated. It is found that, most likely, plasma compression regions between subsequent corotating high-speed streams cause peaks, while heliospheric current sheet crossing causes the majority of the depressions.

Key words: cosmic rays – instrumentation: interferometers – interplanetary medium – solar–terrestrial relations – Sun: heliosphere

1. Introduction

Galactic cosmic rays (GCRs) show an almost isotropic spatial distribution in the inner heliosphere and consist of approximately 90% protons, 8% helium nuclei, 1% heavy nuclei, and 1% electrons (percentages are in particle numbers to the total number). The overall GCR energy integral flux at 1 a.u. ranges approximately from 4000 particles m^{-2} sr^{-1} s^{-1} at solar minimum to 1000 particles m^{-2} sr^{-1} s^{-1} at solar maximum, showing an 11 yr quasi-periodicity (see, for instance, Papini et al. 1996). During periods of negative solar polarity (when the global solar magnetic field lines enter the Sun's North Pole) the flux of positively charged particles appears to

[24] Deceased 2017 April 1.
[25] Deceased 2019 January 20.
[26] Deceased 2012 September 30.

be more modulated up to a maximum of 40% at 100 MeV n^{-1} at solar minimum, with respect to epochs of positive solar polarity (when the global solar magnetic field lines exit the Sun's North Pole, Potgieter 2013). The GCR flux modulation during epochs of opposite solar polarities presents a quasi-periodicity of 22 yr (e.g., Laurenza et al. 2014, and references therein). In addition to these long-term GCR flux modulations, short-term variations ($\leqslant$1 month) associated with the passage of large-scale interplanetary structures are also observed (see for instance Richardson et al. 1996; Sabbah 2000, 2007; Richardson 2004; Sabbah & Kudela 2011; Armano et al. 2018a; Munini et al. 2018).

LISA Pathfinder (*LPF*) was the key technology demonstrator mission of the European Space Agency (ESA) Laser Interferometer Space Antenna (LISA), the first interferometer devoted to gravitational wave detection in space in the frequency interval 10^{-4}–10^{-1} Hz (Amaro-Seoane et al. 2017). The *LPF* spacecraft orbited around the Lagrange point L1 at 1.5 million km from Earth in the Earth–Sun direction. A high counting rate particle detector (PD; Cañizares et al. 2011), hosted on board the *LPF* mission (Antonucci et al. 2011, 2012; Armano et al. 2016, 2018b) allowed for the measurement of the GCR integral proton and helium fluxes above 70 MeV n^{-1} from 2016 February 18 through 2017 July 3 during the descending phase of the present solar cycle N. 24, which characterized by a positive polarity period of the Sun (Grimani et al. 2017; Armano et al. 2018a, 2018c). The aim of placing a PD on board *LPF* was to measure the integral flux of particles of galactic and solar origin that are energetic enough to penetrate the spacecraft and charge the test masses that constitute the heart of the interferometer. Despite the PD not being meant for scientific use, it was tested on a beam experiment (Mateos et al. 2012) and the minimum energy of 70 MeV n^{-1} of ions crossing the detector was measured with high accuracy.

This manuscript focuses on the characteristics of three Forbush decreases (FDs) and of non-recurrent GCR flux short-term variations <2 days observed during the *LPF* mission lifetime. FDs (Forbush 1937, 1954, 1958; Cane 2000) are sudden drops of the GCR flux intensity due to the passage of interplanetary coronal mass ejections (ICMEs) and shocks. These GCR non-recurrent variations have primarily been studied with the world wide neutron monitor (NM) network since the 1950 s (see for instance Barouch & Burlaga 1975; Cane et al. 1996), although only cosmic-ray flux measurements gathered in space (Lockwood 1971) allow for the study of the energy dependence of the depressed GCR flux down to a few tens of MeV without the use of models applied to Earth observations (Beer 2000; Hofer & Flückiger 2000; Usoskin et al. 2011, 2017). The *LPF* 2016 August 2 FD data (Armano et al. 2018a) are compared here to those of the satellite experiment *PAMELA* (Adriani et al. 2011; Usoskin et al. 2015; Munini et al. 2018). The ratio of the depressed to pre-decrease GCR fluxes during the main phase of the observed FDs is studied as a function of the energy.

FD, geomagnetic storm occurrence, and the possibility of using FDs as precursors of geomagnetic activity have previously been studied (see, for instance, Lockwood 1971; Kane 2010; Chauhan et al. 2011; Badruddin & Kumar 2015). FD observations with *LPF* and contemporaneous geomagnetic activity are illustrated here.

The low statistical errors characterizing the data provided by the PD on board *LPF* also allowed for the study of GCR flux non-recurrent variations (depressions and peaks) shorter than 2 days.

This manuscript is organized as follows. In Section 2 the characteristics of the PD hosted on board *LPF* are described. In Section 3 the evolution of three FDs observed with *LPF* are compared to simultaneous measurements of solar wind parameters carried out in L1 and to NM observations placed at different geographic latitudes. In Section 4 parameterizations of proton and helium differential flux measurements gathered in space before and during the main phase of FDs are reported. In Section 5 a brief discussion on FDs and geomagnetic storm occurrence during *LPF* is presented. In Section 6 the association between interplanetary structures and <2 day GCR flux non-recurrent variations is illustrated.

2. The PD on board the *LPF* Spacecraft

The *LPF* spacecraft was launched with a Vega rocket from the Kourou base in French Guiana on 2015 December 3. The satellite reached its final 6 month orbit around the first Lagrangian point L1 at the end of 2016 January. The spacecraft elliptical orbit was inclined by about 45° to the ecliptic. The minor and major axes of the orbit were approximately 0.5 million km and 0.8 million km, respectively.

Two nearly 2 kg cubic gold–platinum free-falling test masses served as the mirrors of the interferometer on board *LPF*. Cosmic rays with energies larger than 100 MeV n^{-1} penetrated approximately 13 g cm^{-2} of the spacecraft and instrument materials and charged the test masses. This process was expected to constitute one of the main sources of noise for LISA-like space interferometers in case of intense solar energetic particle (SEP) events (Shaul et al. 2006; Armano et al. 2017). A PD on board *LPF* allowed for in situ monitoring of protons and helium nuclei of GCRs and solar particles. A shielding copper box of 6.4 mm thickness surrounded the silicon wafers in order to stop ions with energies smaller than 70 MeV n^{-1}. This conservative choice was made in order not to underestimate the overall incident particle flux charging the test masses.

The *LPF* PD was mounted behind the spacecraft solar panels with its viewing axis along the Sun–Earth direction. It consisted of two ~300 μm thick silicon wafers of 1.40 × 1.05 cm^2 area, placed in a telescopic arrangement at a distance of 2 cm. This detector allowed for the counting of particles traversing each of the two silicon layers (single counts). Single counts were returned to the telemetry every 15 s. The energy deposits in the rear detector of particles traversing both silicon wafers in less than 525 ns (coincidence mode) were stored on the onboard computer in histograms of 1024 energy linear bins from 0 MeV to 5 MeV and returned to the telemetry every 600 s. The PD geometrical factor for particle energies >100 MeV n^{-1} was of 9 cm^2 sr for single counts and about one-tenth of this value for particles in coincidence mode. The maximum allowed detector counting rate was 6500 counts s^{-1} in the single count configuration. In coincidence mode 5000 energy deposits per second was the saturation limit corresponding to an event proton fluence of 10^8 protons cm^{-2} at energies >100 MeV.

The spurious test-mass acceleration noise due to the charging process was estimated before the mission launch with Monte Carlo simulations (Araújo et al. 2005; Grimani et al. 2005, 2015; Wass et al. 2005) on the basis of GCR and SEP flux predictions

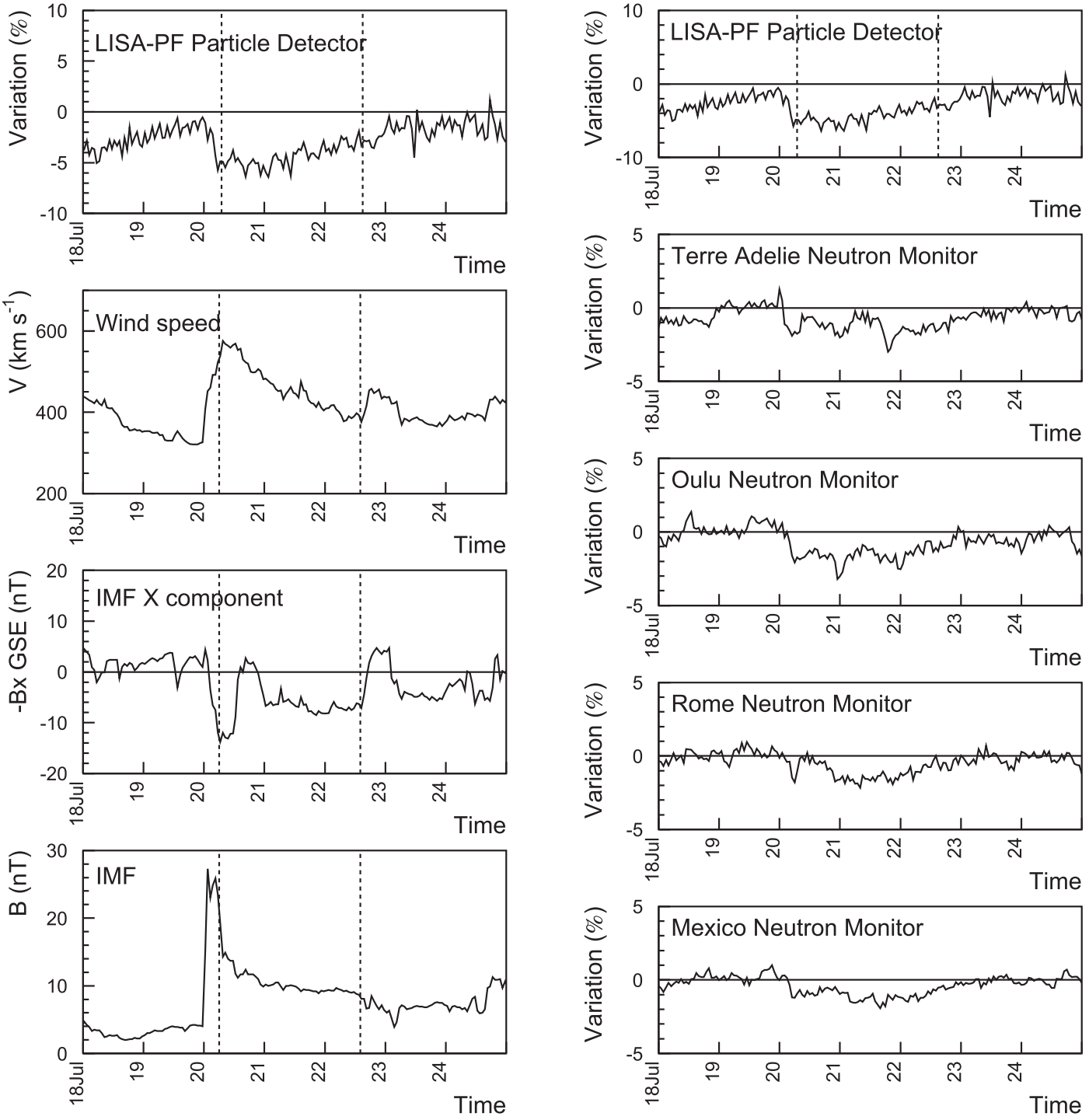

Figure 1. Left: the *LPF* PD GCR hourly averaged counting rate PC between 2016 July 18 and 2016 July 24 are reported in the top panel. The solar wind speed (V) is shown in the second panel. The Geocentric Solar Ecliptic (GSE) coordinate system sunward IMF x-component with the opposite sign ($-B_x$) and IMF intensity (B) appear in the third and fourth panels, respectively. The IMF and solar wind parameter data were gathered from the *ACE* experiment (https://cdaweb.sci.gsfc.nasa.gov/index.html) at Lagrange point L1. The passage of a near-Earth ICME is indicated by vertical dashed lines (http://www.srl.caltech.edu/ACE/ASC/DATA/level3/icmetable2.htm). A FD is observed to begin on July 20. Right: comparison of *LPF* hourly averaged GCR counting rate PC with contemporaneous, analogous measurements of NMs placed at various geographic latitudes (www.nmdb.eu). The dashed lines in the top panel have the same meaning as those in the left figures.

at the time the mission was supposed to be sent into orbit. The reliability of GCR flux predictions was positively tested with *LPF* data after mission end (Armano et al. 2018c) and with the Space Station AMS-02 magnetic spectrometer experiment (Aguilar et al. 2002) preliminary data above 400 MeV n^{-1} presented at COSPAR 2018 (2018 July 14–22, Pasadena, USA) and expected to be reported in a forthcoming publication of the AMS collaboration. No SEP events occurred during the *LPF* mission, nevertheless test-mass discharging was carried out periodically with ultraviolet light beams illuminating the capacitor system surrounding the test masses (Armano et al. 2017, 2018d) for acceleration noise control.

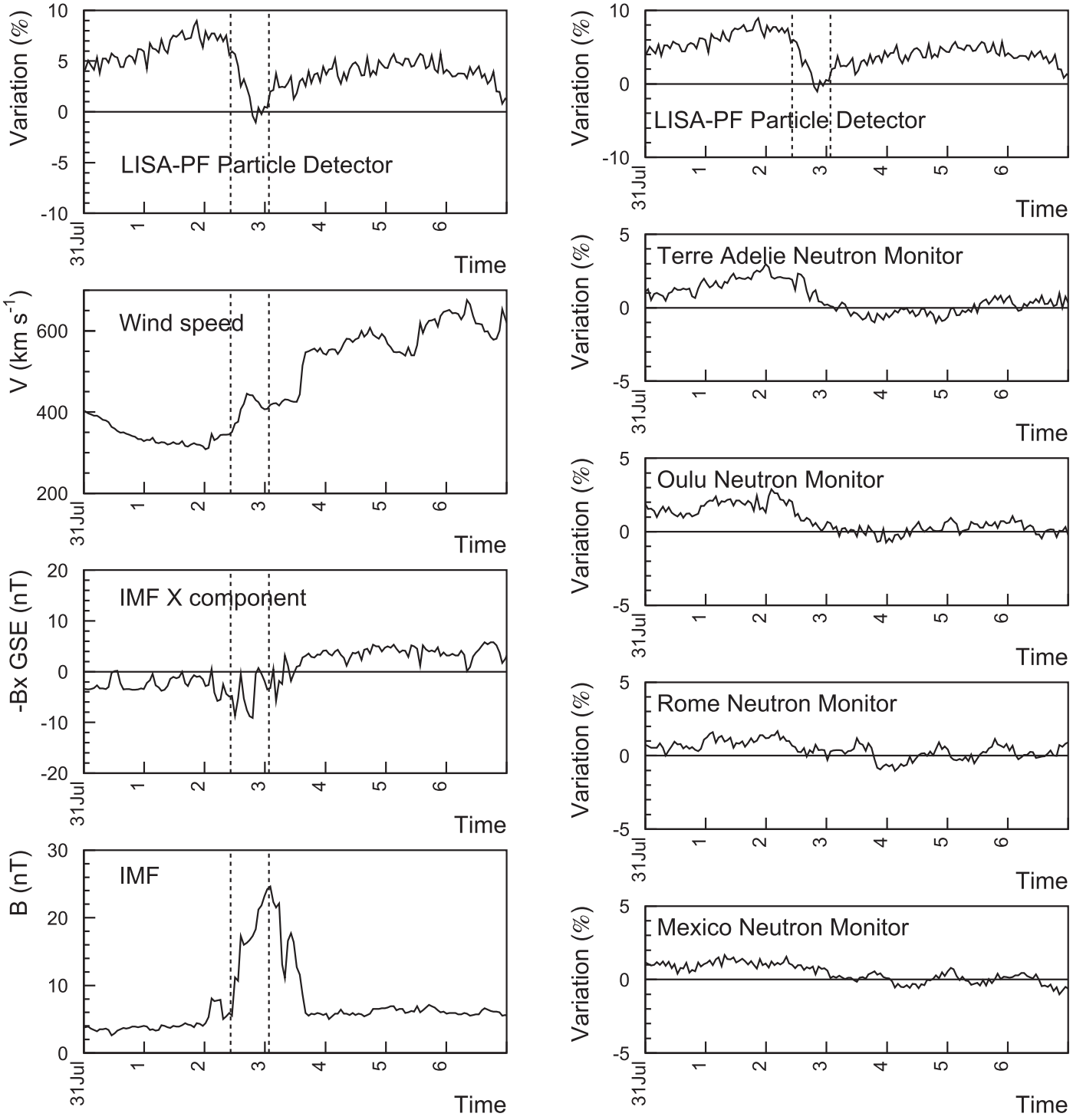

Figure 2. Same as Figure 1, but for the period 2016 July 31–2016 August 6.

3. Characteristics of FDs Observed with *LPF*

The *LPF* 15 s proton and helium single counts gathered between 2016 February 18 and 2017 July 3 were hourly averaged in order to set the statistical uncertainty of each data point to 1%. The percentage change (PC) of these measurements calculated with respect to their average value observed during each Bartels rotation (BR) was visually inspected over the *LPF* mission lifetime. This approach was adopted in order to limit the role of the solar modulation decrease during the years 2016–2017. It is recalled here that the BR number represents the number of 27 day periods of the Sun since 1832 February 8. The GCR flux variations were then compared to contemporaneous interplanetary magnetic field (IMF) and solar wind plasma parameters gathered by the *ACE* experiment (Stone et al. 1998) orbiting around the Lagrange point L1 (https://cdaweb.sci.gsfc.nasa.gov/index.html).

The passage of near-Earth ICMEs (reported in http://www.srl.calctech.edu/ACE/ASC/DATA/level3/icmetable2.htm) was associated with three FD observations carried out with the *LPF* PD on 2016 July 20, 2016 August 2 (for this event see also

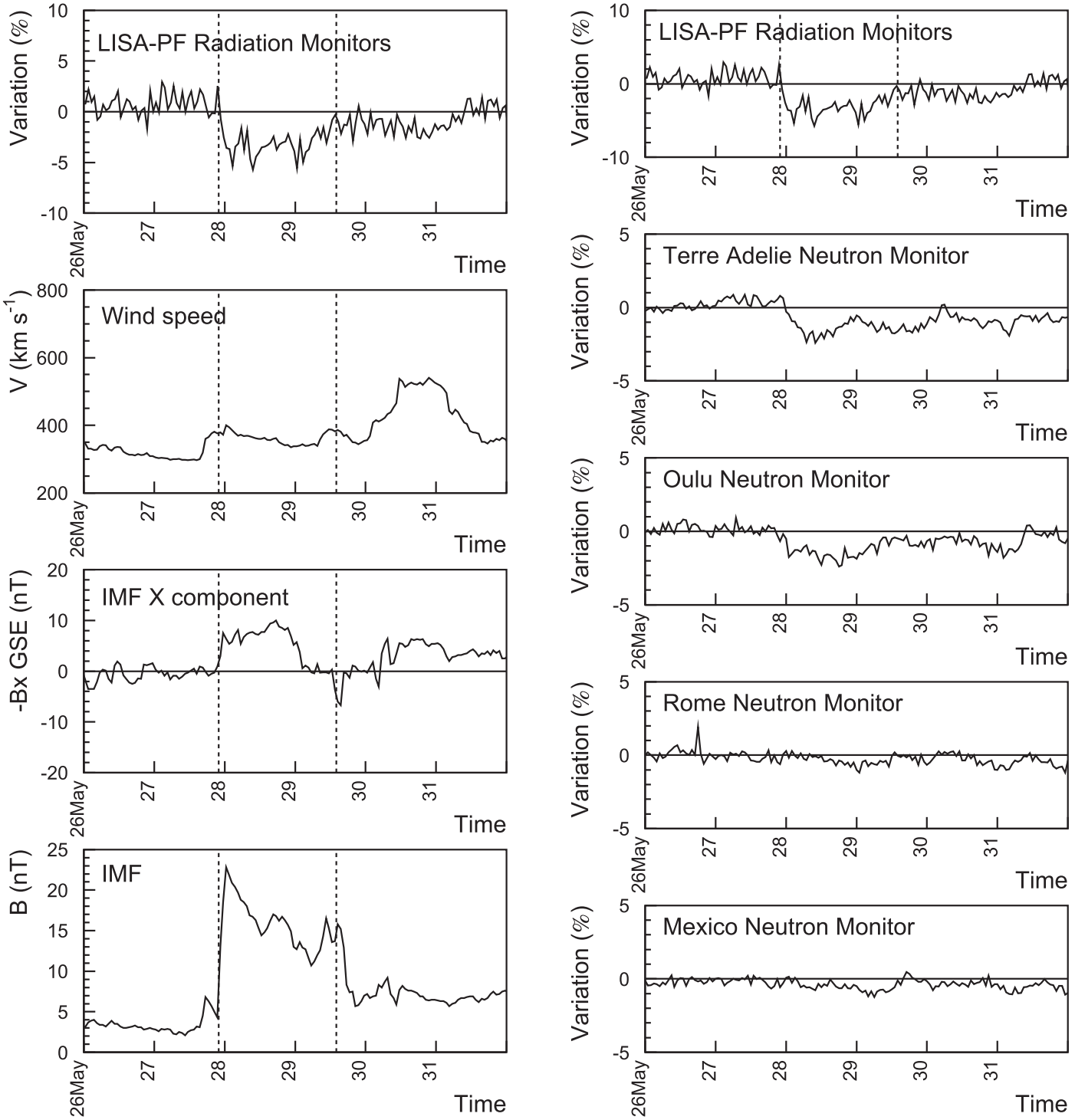

Figure 3. Same as Figure 1, but for the period 2017 May 26–31.

Armano et al. 2018a) and 2017 May 27, as s shown in the left panels of Figures 1–3. In these figures the GCR flux variations are compared to the solar wind speed (V), to the IMF sunward x-0component in the GSE coordinate system with the opposite sign ($-B_x$) observed to match the sector polarity, and to the IMF intensity (B). The ICME passage is marked with dashed lines. The FD dated 2016 July 20 is associated with both solar wind speed and IMF increases due to the ICME propagating into a previous corotating high-speed solar wind stream (CHSS, $V \gg 400\,\mathrm{km\,s^{-1}}$). On 2016 August 2 and 2017 May 27 the GCR flux modulations appear correlated with the IMF intensity increase only. In all three cases the IMF intensity presented maximum values of about 25 nT.

In order to study the energy dependence of the three FDs observed with *LPF*, the PCs of the integral proton and helium fluxes measured with the PD above 70 MeV n^{-1} were compared to contemporaneous hourly averaged PCs of observations gathered with NMs located at different geographic latitudes in the right panels of Figures 1–3 (www.nmdb.eu, a similar attempt for NMs only was carried out in Badruddin & Kumar 2015). The

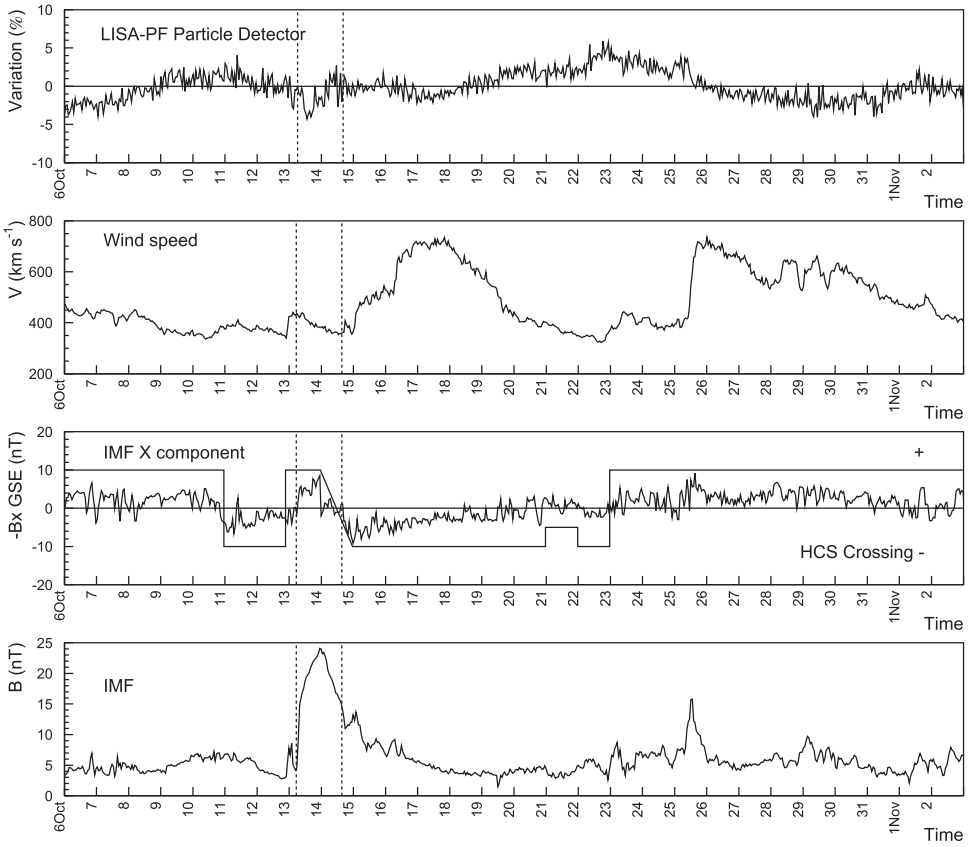

Figure 4. From top to bottom: GCR flux variations on board *LPF*; solar wind speed (V), IMF negative component ($-B_x$) in a GSE coordinate system and IMF intensity (B) during the BR 2499 (2016 October 6–2016 November 1). In the third panel the continuous line indicates HCSC and the sector daily polarity (positive and negative polarities were set to +10 and −10 arbitrarily in the plot). Undefined polarities were equally arbitrarily set to +5 and −5 (sector polarities are available at http://omniweb.sci.gsfc.nasa.gov./html/polarity/polarity_tab.html). The passage of a near-Earth ICME is indicated by the vertical dashed lines (http://www.srl.caltech.edu/ACE/ASC/DATA/level3/icmetable2.htm).

Table 1
Energy Dependence of the GCR Integral Flux PC at the Maximum of the Three FDs Observed on board *LPF* above 70 MeV n^{-1} and with NMs above Effective Energies: 11 GeV for Polar Stations; 12 GeV for Oulu NM; 17 GeV for Rome NM, and 20 GeV for Mexico NM

LPF FD Onset Time	*LPF* FD Maximum Time	PC >70 MeV	PC >11 GeV	PC >12 GeV	PC >17 GeV	PC >20 GeV
2016 Jul 20 07.00 UT	Jul 21 01.00 UT	5.5%	2%	2%	2%	1%
2016 Aug 2 12.00 UT	Aug 2 22.40 UT	9%	3%	2%	2%	1%
2017 May 27 18.00 UT	May 28 10.45 UT	7%	3.5%	2.5%	1%	1%

GCR flux PCs observed on board *LPF* or with NMs were calculated with the baseline (PC = 0%) being the average values of counts measured by PD or NMs during the BR to which the studied period of time belongs. The Terre Adelie, Oulu, Rome and Mexico NM stations are characterized by geomagnetic cutoff rigidities of 0 GV, 0.8 GV, 6.3 GV and 8.2 GV, respectively. The shielding effect of the atmosphere and the geomagnetic cutoff do not allow NMs to provide direct measurements of GCR energy spectra at low energies. Conversely, the PC of the NM counting rate measured on Earth is approximately the same as the GCR integral flux incident at the top of the atmosphere above *effective energies*. Effective energies range from 11 to 12 GeV for polar stations, to 20 GeV for equatorial stations (for more details, see Gil et al. 2017, and references therein). Table 1 provides the PC of the GCR integral flux observed with *LPF* and with the NMs listed above, at the maximum of each FD. The time of the onset and the maximum of each FD on board *LPF* are also indicated. The onset was set as the first time bin after which the GCR flux presented a continuous decreasing trend, within statistical uncertainty, for at least six hours. The time when the GCR integral flux reached its minimum value during each FD was estimated with a best line fit through the data points. The *LPF* proton-dominated (resulting from proton and helium measurements) integral flux maximum decreases above 70 MeV were observed to vary from about 5% to 9% during the three events. The different GCR flux decrease observed with *LPF* in response to similar IMF intensity increases is most likely due to the passages of interplanetary structures that depressed the GCR flux before the transit of the ICMEs. During the 2016 August 2 event only, the pre-decrease GCR flux appeared at its maximum value during the BR 2496 before the passage of the ICME that generated the FD (see Figure 7 in Armano et al. 2018a). NM data show PCs above effective energies ranging between 1% and 3%. Both GCR flux main and

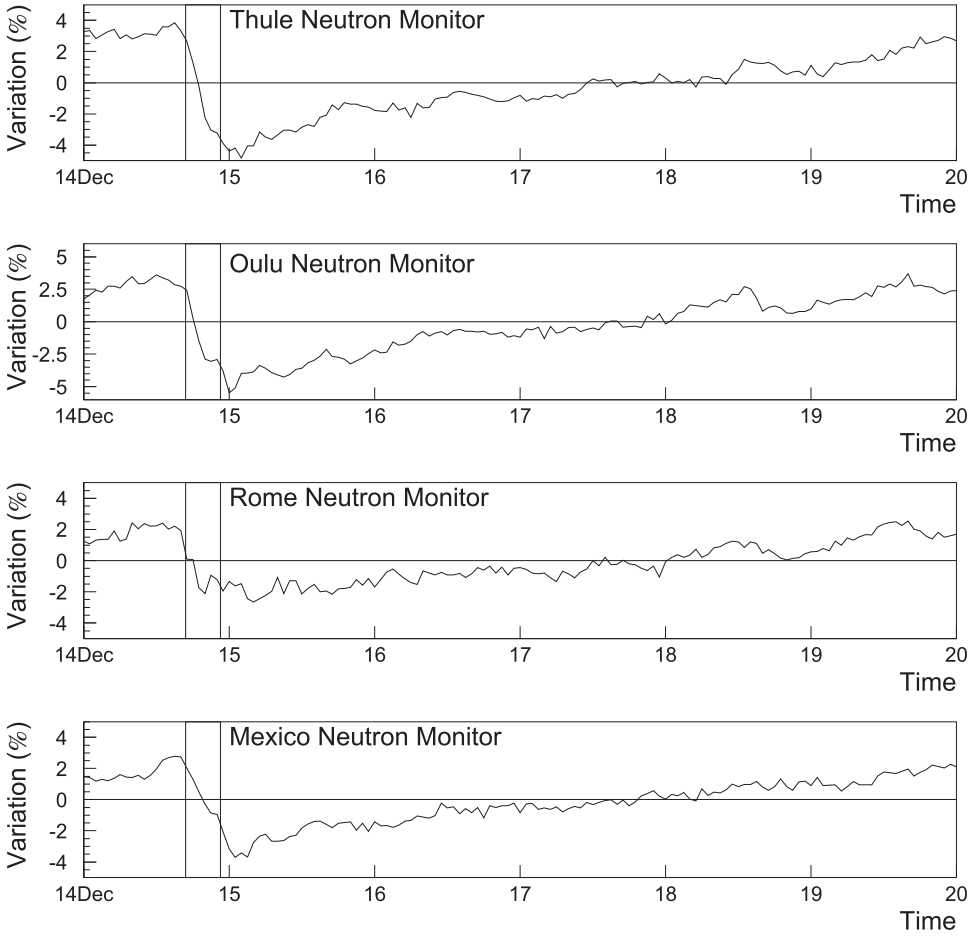

Figure 5. NM measurements at various geographic latitudes between 2006 December 14 and 19. An FD on December 14 was also observed in space by *PAMELA* above 70 MeV n^{-1} from 16.50 UT through 22.35 UT on 2006 December 14 (vertical continuous lines).

recovery phases are observed in all considered NM measurements during the 2016 July 20 FD. This is not the case for the other two events that can be clearly detected in polar NM measurements only. The energy dependence of GCR flux depressions during FDs was also discussed, for instance, in Usoskin et al. (2008), Grimani et al. (2011), and Badruddin & Kumar (2015).

The transits of the other three near-Earth ICMEs on 2016 March 5, 2016 April 14 and 2016 October 13 resulted in GCR flux decreases at the limit of the statistical significance (1%–2%) on *LPF*, as the GCR flux was already reduced by the transits of previous interplanetary structures and the heliospheric current sheet crossing (HCSC; see Figure 6 in Armano et al. 2018a and Figure 4).

4. Parameterization of GCR Energy Spectra during FDs

GCR flux measurements gathered in space are considered to investigate if the same parameterization could be used to replicate the trend of the GCR flux PC during the main phases of FDs of different intensities. The *LPF* GCR observations gathered before and at the maximum (22.40 UT) of the 2016 August 2 FD are compared to those of the satellite *PAMELA* experiment, which measured both proton and helium differential fluxes before and during the main phase of the FD dated 2006 December 14 between 16.50 UT and 22.35 UT (see for details Adriani et al. 2011; Usoskin et al. 2015; Munini et al. 2018). The *PAMELA* data can be found in https://tools.ssdc.asi.it/CosmicRays/. In Figure 5 vertical solid lines delimit the interval of time during which *PAMELA* observed the FD. The pre-decrease and depressed proton energy spectra observed by *PAMELA* in 2006 November and on 2006 December 14, respectively, are shown in Figure 6. The *PAMELA* data are reported in https://tools.ssdc.asi.it/CosmicRays/. In the same figure, pre-decrease and depressed proton-dominated energy differential fluxes for the FD dated 2016 August 2 are also reported.

The *PAMELA* data gathered during the main phase of the FD are not shown below 500 MeV because the proton flux included particles of both galactic and solar origins. Note that the *PAMELA* pre-decrease flux measurements were considered those gathered in 2006 November becausee the solar modulations during the months of 2006 November and 2006 December were very similar (http://cosmicrays.oulu.fi/phi/Phi_mon.txt). *PAMELA* helium data for the same FD appear in Figure 7.

The energy spectra of cosmic rays observed during the main phase of the FDs ($F_{FD}(E)$) considered in this section and corresponding pre-decrease energy spectra ($F(E)$) are parameterized as indicated in Equations (1) and (2) (Papini et al. 1996), respectively:

$$F_{FD}(E) = A\ (E + b')^{-\alpha}\ E^{\beta}\ \text{particles}\ (\text{m}^2\ \text{sr}\ \text{s}\ \text{GeV}\ \text{n}^{-1})^{-1}, \quad (1)$$

$$F(E) = A\ (E + b)^{-\alpha}\ E^{\beta}\ \text{particles}\ (\text{m}^2\ \text{sr}\ \text{s}\ \text{GeV}\ \text{n}^{-1})^{-1}, \quad (2)$$

Table 2
Parameterizations of Proton (p) and Helium (He) Energy Spectra Measured by the Indicated Experiments Before and During Forbush Decreases (See Equations (1) and (2))

	A	b	b'	α	β	χ^2	$n$dof
p (PAMELA Experiment—2006 Nov)	18,000	1.17	⋯	3.66	0.87	2279.1	71
p (FD—2006 Dec 14 16.50 UT–22.35 UT)	18,000	⋯	1.37	3.66	0.87	4948.7	71
p (*LPF*—2016 Aug)	18,000	1.10	⋯	3.66	0.87	⋯	⋯
p (2006 Aug 2 22.40 UT)	18,000	⋯	1.17	3.66	0.87	⋯	⋯
He (PAMELA Experiment—2006 Nov)	850	0.75	⋯	3.47	0.72	16.38	18
He (FD—2006 Dec 14 16.50 UT–22.35 UT)	850	⋯	0.90	3.47	0.72	10.98	18

Note. The χ^2 and number of degrees of freedom ($n$dof) estimated for each set of experimental data are indicated.

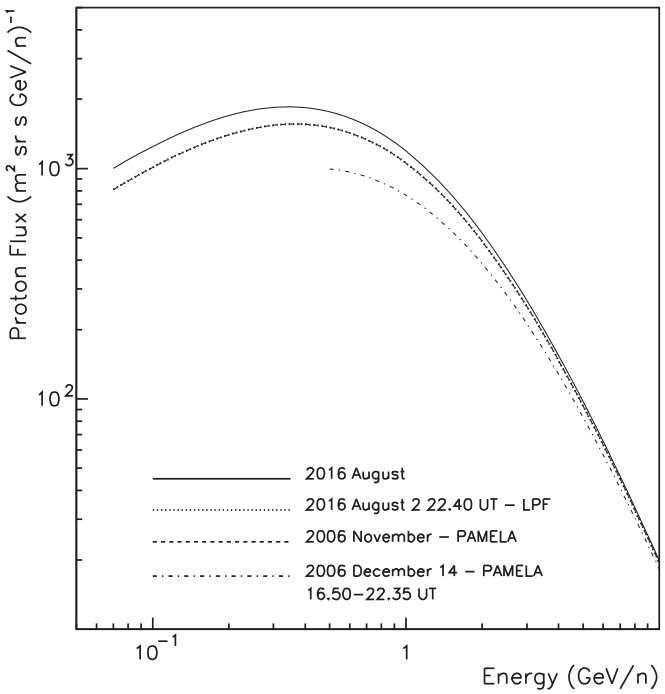

Figure 6. Proton energy spectra measured by *PAMELA* before (dashed line) and during the FD dated 2006 December 14 (dotted-dashed line). The proton-dominated observations carried out with *LPF* and NMs on 2016 August 2 at the maximum of the FD (22.40 UT) are also shown (dotted line). The 2016 August pre-decrease proton flux is represented by a continuous line. The depressed proton spectrum observed during the August 2 FD with *LPF* is superposed on the pre-decrease proton flux measured by *PAMELA* in 2006 November.

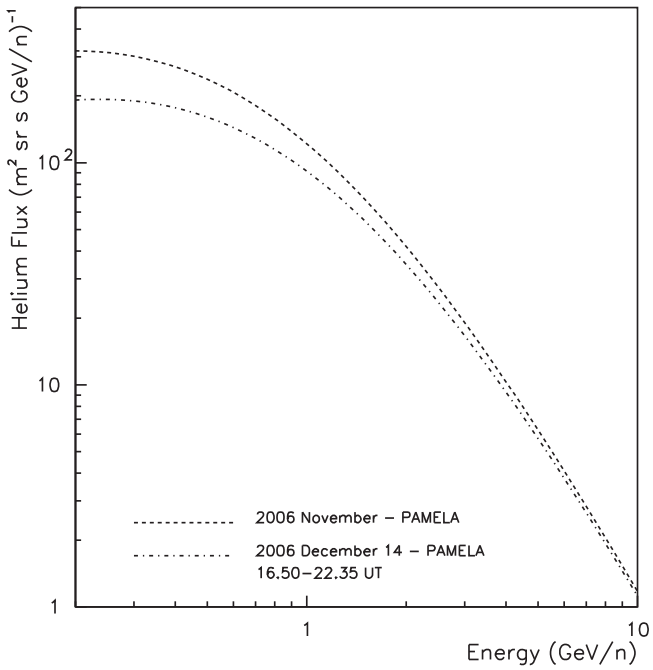

Figure 7. Helium energy spectra measured by *PAMELA* before and during the FD dated 2006 December 14.

with $b' > b$. The parameters α and β remain unchanged because these parameters modulate the GCR flux above 10 GeV, where pre-decrease and depressed fluxes present approximately the same slope observed in Figures 6 and 7. The parameterizations reported in Equations (1) and (2) are found to reproduce the GCR energy spectra trend in the inner heliosphere in an energy range of observations between a few tens of MeV n^{-1} up to hundreds of GeV n^{-1}, in agreement with the Gleeson and Axford model (Gleeson & Axford 1968), within experimental errors of data. These parameterizations are adopted in this work instead of using the model by Gleeson and Axford during FDs (see, for instance, Usoskin et al. 2015), because in this last model the modulation of GCR energy spectra is correlated with the solar modulation parameter that follows the long-term quasi-periodicity of the solar activity. The solar modulation parameter is kept constant during each BR and it is preferred to increase the parameter b (in Equation (2)) to b' (in Equation (1)) to reproduce the observed GCR flux trend during an FD to decouple the effects of long-term and short-term GCR flux variations.

The parameters A, b, b', α, β estimated for each data set are indicated in Table 2. The χ^2 and number of degrees of freedom for each parameterization of the *PAMELA* data (available in https://tools.ssdc.asi.it/CosmicRays) are also reported in Table 2. For the 2016 August 2 *LPF* FD the pre-decrease proton differential flux above 70 MeV was estimated on the basis of the Gleeson and Axford model by assuming a solar modulation parameter of 438 MV (http://cosmicrays.oulu.fi/phi/Phi_mon.txt) for 2016 August and the interstellar proton spectrum by Burger et al. (2000). The differential flux thus obtained was then parameterized as indicated in Equation (2) and integrated above 70 MeV and above the effective energies of polar, Oulu, Rome, and Mexico NM stations. The integral flux values were then reduced at 70 MeV and at effective energies as observed by *LPF* at 22.40 UT of 2016 August 2 and by NMs between 22.00 and 23.00 UT on the same day. Finally, the differential flux at the maximum of the FD was estimated by increasing the parameter b of the pre-decrease differential flux (third row in Table 2 and Equation (2)) to b' (fourth row in

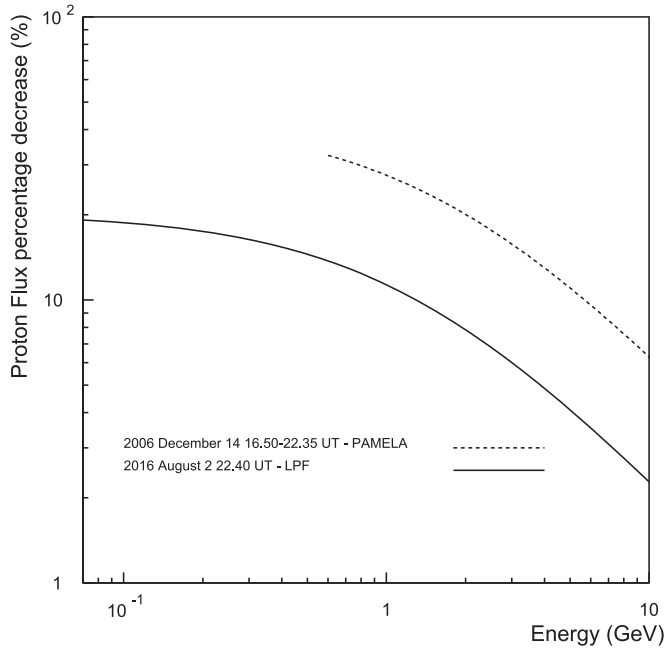

Figure 8. Parameterization of the proton flux percentage decrease observed by PAMELA and *LPF* during the main phase of the FDs dated on 2006 December 14 and 2016 August 2, respectively.

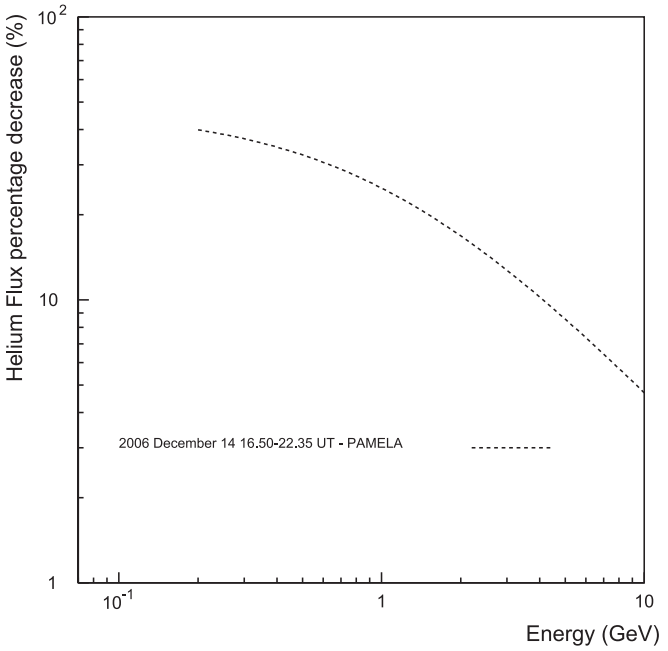

Figure 9. Parameterization of the percentage decrease of the helium flux observed by the *PAMELA* experiment during the FD dated on 2006 December 14.

Table 2 and Equation (1)) until obtaining an agreement to better than 1% between the modulated integral flux and integral flux measurements carried out with *LPF* and NMs. No χ^2 was calculated for *LPF* because no differential flux measurements are available for our experiment. In Armano et al. (2018a) the same approach presented here was adopted using the Shikaze et al. (2007) interstellar proton spectrum inferred from the BESS experiment data gathered during both the positive and negative polarity periods of the Sun. The solar modulation parameter values obtained with the BESS data differ from those reported in http://cosmicrays.oulu.fi/phi/Phi_mon.txt, which were obtained with the Burger et al. (2000) interstellar spectra only by a few tens of MV, which can be considered to lie within the uncertainty of the method. After the publication of the AMS experiment data gathered during 2016 August, it will be possible to set the uncertainties on the outcomes of the present work.

By defining $R(E)$ the ratio of the GCR flux interpolations that appear in Equations (1) and (2), respectively,

$$R(E) = \frac{F_{\rm FD}(E)}{F(E)}, \tag{3}$$

it is found that

$$R(E) = \left(\frac{E + b'}{E + b}\right)^{-\alpha}. \tag{4}$$

The $R(E)$ estimated for *LPF* and *PAMELA* proton measurement interpolations are shown in Figure 8, while in Figure 9, $R(E)$ were calculated for the *PAMELA* helium observation interpolations. The simple relationship in Equation (3) allows for a quick (albeit approximate) estimate of the GCR energy differential flux during the main phase of an FD when integral flux measurements during the event evolution and the differential flux before the occurrence of the same are known.

The b/b' ratios of the parameters estimated with the GCR flux parameterizations before and during the main phase of each FD studied in this section (two data points were considered for the FD from 2006 December 14 because *PAMELA* measured both proton and helium fluxes) appear correlated with the GCR flux percentage attenuation (PA), as is shown in Figure 10 (solid dots). PA is defined as follows

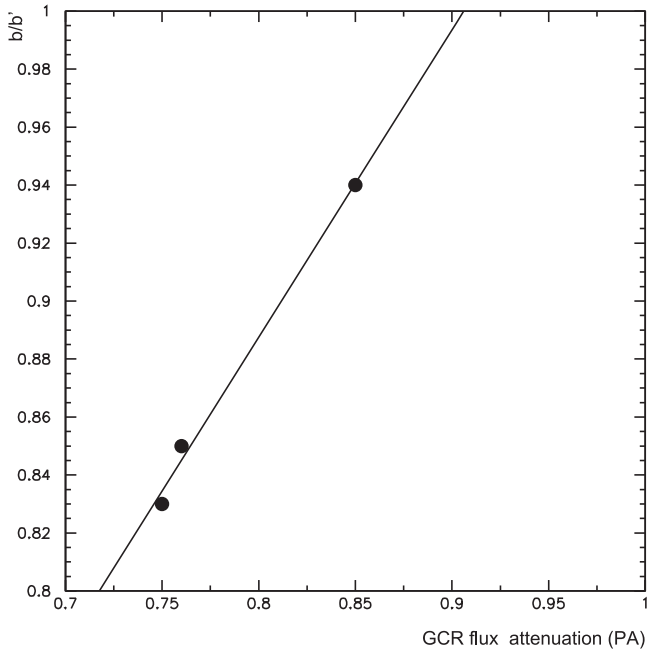

Figure 10. Parameterization of the b/b' ratio inferred from Equations (1) and (2) for the FDs studied in this section vs. the GCR flux percentage attenuation (PA). The continuous line indicates the best fit of the data points: $b/b' = 1.061$ PA+0.0387.

$$\mathrm{PA} = \frac{\int F_{\rm FD}(E)dE}{\int F(E)dE}, \tag{5}$$

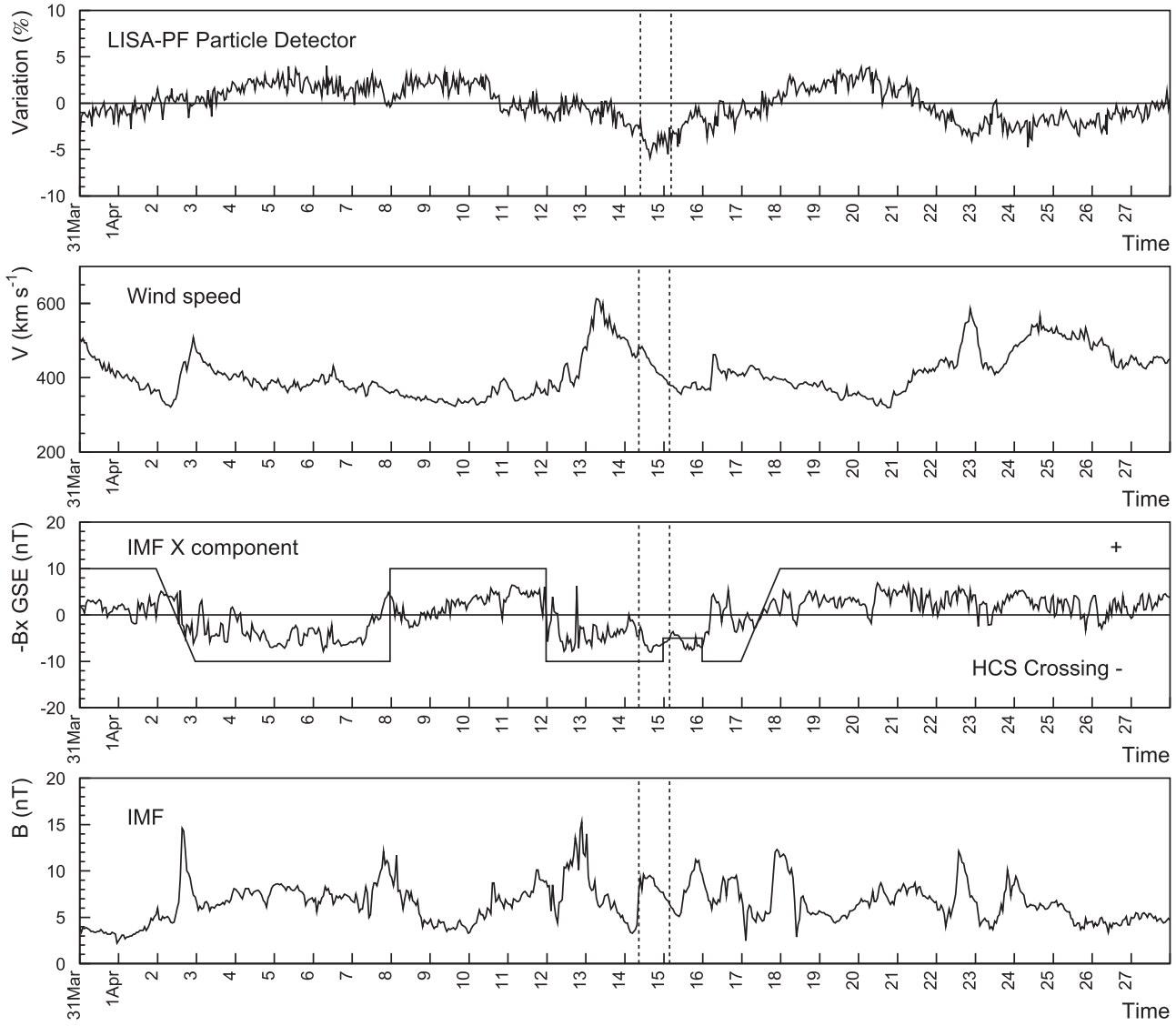

Figure 11. Same as Figure 4, but for the BR 2492 (2016 March 31–2016 April 26).

where integrals are calculated in the energy range of data available during each event.

In Figure 11 the continuous line indicates the best fit through the data points. If additional observations gathered in space will confirm the reliability of this simple empirical relationship, it will be possible to set the statistical significance.

5. FD Observations at Lagrange Point L1 and Geomagnetic Storm Occurrence

Fifteen near-Earth ICMEs were observed (http://www.srl.caltech.edu/ACE/ASC/DATA/level3/icmetable2.htm) as *LPF* was orbiting around Lagrange point L1. Eight of these ICMEs had magnetic clouds. As was anticipated in Section 3, the GCR integral flux measurements on board *LPF* presented depressions at the time of the passage of six of these ICMEs (2016 March 5; 2016 April 14; 2016 July 20; 2016 August 2, 2016 October 13 and 2017 May 27), but only in three cases (on 2016 July 20, 2016 August 2 and 2017 May 27) were FDs observed. During the main phases of these three FDs the GCR flux decreases appeared correlated with the increase of the IMF intensity up to about 25 nT associated with the contemporaneous transit of ICMEs (see also Benella et al. 2019), while the solar wind speed remained below 400 km s^{-1} except at the onset of the 2016 July 20 event. Conversely, during the GCR flux depressions observed on 2016 March 5 (Figure 6 in Armano et al. 2018a) and 2016 April 14 (Figure 11) the effects of ICME passages (from 19.00 UT on March 5 through 15.00 UT on March 6 and 09.00 UT on April 14 through 04.00 UT on April 15, respectively) were mainly concealed by the action of concomitant transits of several CHSS. On 2016 October 13 the role of a near-Earth ICME passage (from 2016 October 13 at 6.00 UT through 2016 October 14 at 16.00 UT; dashed lines in Figure 4) and the increase of the IMF intensity >20 nT in modulating the GCR flux could not be established because the GCR flux presented a continuous decreasing trend well before the passage of the ICME due to a previous transit of high-speed solar wind streams and HCSC on October 11, 13, and 14.

Geomagnetic storms are disturbances of the Earth's magnetosphere classified on the basis of their intensity by changes in the Dst (disturbance storm time) geomagnetic index representing the average change of the horizontal component of the Earth's

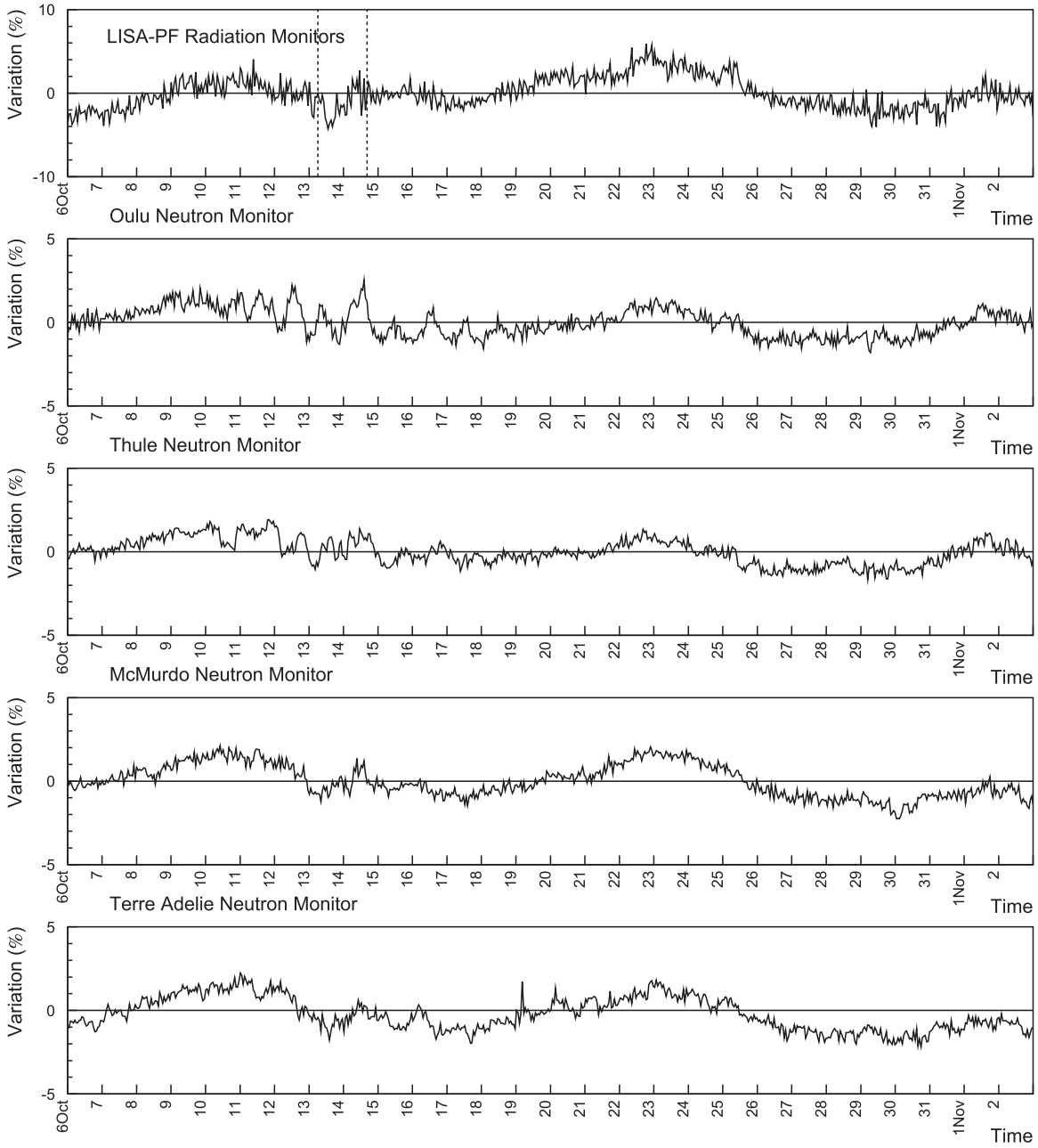

Figure 12. Comparison of *LPF* hourly averaged GCR counting rate PC (top panel) with contemporaneous, analogous measurements of polar NMs during the BR 2499 (2016 October 6–2016 November 1). The passage of a near-Earth ICME is indicated by vertical dashed lines (http://www.srl.caltech.edu/ACE/ASC/DATA/level3/icmetable2.htm).

Table 3
FD Observations and Geomagnetic Storm Occurrence During the *LPF* Mission

Date	FD Yes/No	Geomagnetic Storm Yes/No	Maximum B nT	Minimum B_z nT	Dst nT
2016 Jul 20	Yes	No	25	−8.9	>-50
2016 Aug 2	Yes	No	24	−9.5	$\simeq-50$
2016 Oct 13	No	Yes	24	−19	−102
2017 May 27	Yes	Yes	23	−21	−122

magnetic field at the magnetic equator (Gonzales et al. 1994). Geomagnetic storms are defined as weak when the Dst ranges between −30 and −50 nT; moderate when the Dst varies between −50 and −100 nT; and strong when the Dst is smaller than −100 nT. Moderate geomagnetic storms, which are more frequent than strong ones, affect communications, while the most intense ones may severely damage critical Earth infrastructure. Near-Sun coronal mass ejection and near-Earth solar wind parameters are used to forecast geomagnetic storms (Kim et al. 2014). The geomagnetic index Dst reached a value smaller than −100 nT

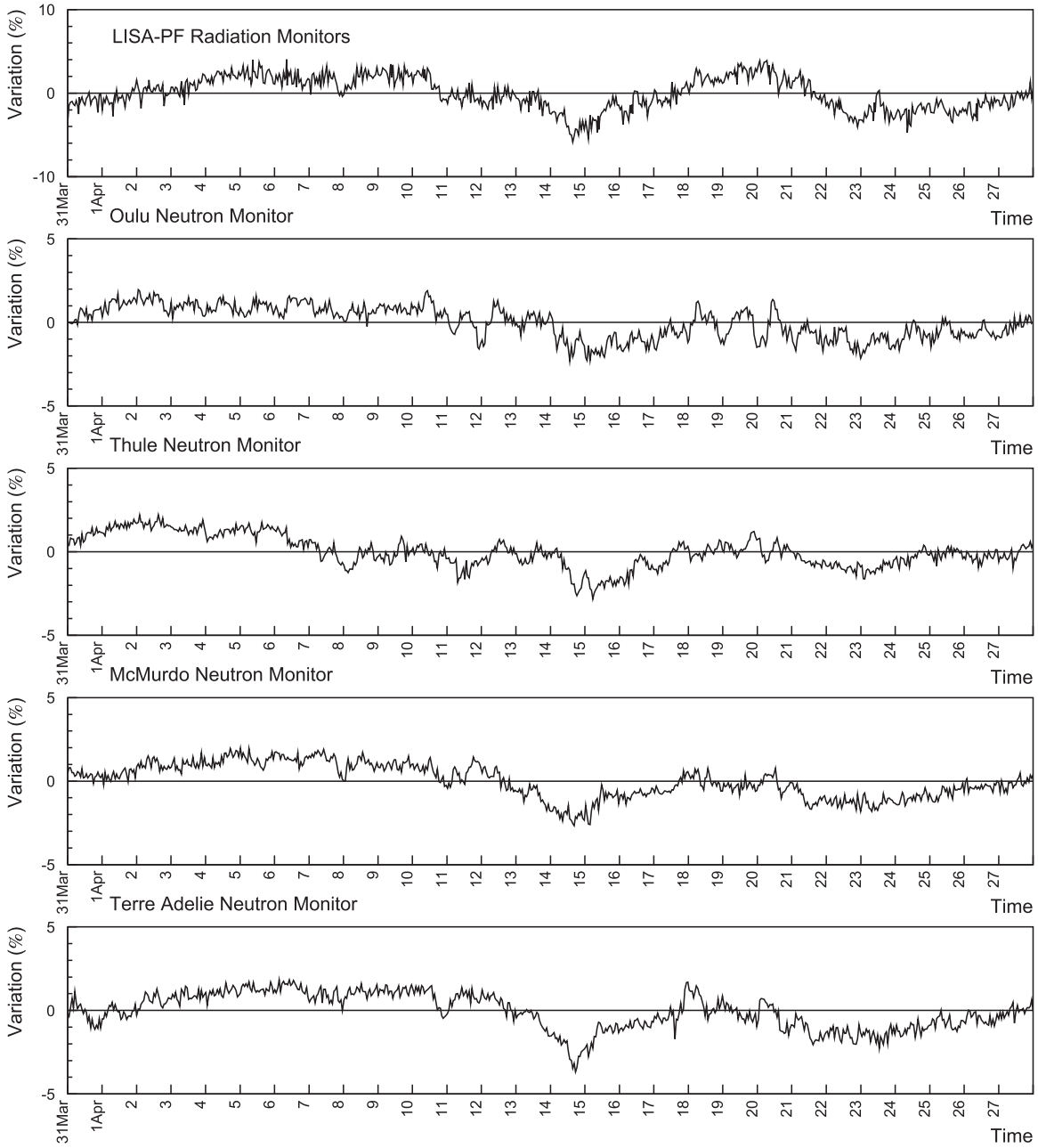

Figure 13. Same as Figure 13, but for the BR 2492 (2016 March 31–2016 April 26).

twice during the period in which *LPF* collected data (2016 February 18–2017 July 3): on 2016 October 13 at 17.30 UT (−104 nT) and on 2017 May 28 at 07.30 UT (−122 nT). In Figure 12 it is shown that no FD can be observed beyond statistical fluctuations with *LPF* and NMs. Conversely, the passage of a near-Earth ICME was at the origin of both the FD observed on *LPF* and NMs on 2017 May 27–28 (Figure 3) and the geomagnetic storm that occurred on 2017 May 28. The 2016 August 2 FD onset occurred at 12.00 UT on board *LPF*, about 10 hours before a weak geomagnetic storm (Dst $\simeq -50$ nT) that started at 22.00 UT when the FD reached its maximum ate Lagrange point L1 (see Figure 7 in Armano et al. 2018a). For this event the geomagnetic storm and the maximum of the FD occurred at the same time even though this is not a general result (see Kane 2010, for instance). Geomagnetic storms are caused by fast solar wind streams and large negative values of the B_z component of the IMF reconnecting with the Earth's magnetic field, while FDs are caused by large increases of the IMF intensities. FD observations with *LPF* at Lagrange point L1 and geomagnetic storm occurrence are summarized in Table 3 along with maximum values of the observed IMF intensity and minimum values of the B_z component during each FD. It can be concluded that FDs, when observed, can be used to forecast geomagnetic storms only when the z-component of the IMF presents values <-20 nT (see also Dremukhina et al. 2011).

6. GCR Flux Non-recurrent Variations <2 Days During *LPF*

A visual data inspection of the whole *LPF* data set revealed the presence of several non-recurrent substructures in the GCR flux that lasted less than two days. A dedicated analysis was carried

Table 4
Occurrence and Characteristics of the GCR Flux Variations <2 Days Observed with *LPF*

Date	Onset Time	Duration Days	Dip/Peak	Amplitude %	Interplanetary Structure
2016 Mar 11	7.44 UT	0.97	DIP	3.1	CIR+HCSC
2016 Mar 16	1.38 UT	0.84	PEAK	3.0	MB
2016 Mar 19	9.21 UT	1.16	DIP	2.5	CHSS
2016 Apr 7	16.31 UT	0.89	DIP	3.4	HCSC
2016 Apr 15	7.44 UT	0.75	PEAK	4.4	MB
2016 Apr 23	1.13 UT	1.16	PEAK	3.0	MB
2016 Jun 16	0.15 UT	1.74	PEAK	2.5	MB
2016 Jun 21	23.11 UT	1.68	DIP	2.5	HCSC
2016 Jun 23	2.12 UT	1.95	DIP	2.5	CIR
2016 Jun 25	6.55 UT	1.79	DIP	2.5	CHSS
2016 Jun 30	7.19 UT	1.79	DIP	2.8	HCSC
2016 Jul 2	3.15 UT	2.00	DIP	2.8	MFE
2016 Jul 4	8.57 UT	1.74	DIP	2.5	CHSS+HCSC
2016 Aug 9	00.30 UT	0.75	PEAK	4.4	MB
2016 Aug 16	6.06 UT	1.79	DIP	2.5	HCSC
2016 Sep 15	22.43 UT	0.84	DIP	3.1	MFE
2016 Oct 11	13.25 UT	0.95	DIP	2.5	CHSS
2016 Oct 23	21.09 UT	0.95	DIP	3.8	HCSC+CHSS
2016 Nov 10	17.29 UT	1.16	DIP	3.8	CIR+HCSC
2017 Jan 14	12.52 UT	0.75	DIP	3.1	HCSC
2017 Mar 22	22.21 UT	1.05	PEAK	2.1	MB
2017 May 5	12.17 UT	1.46	DIP	2.3	MFE
2017 May 29	21.07 UT	1.53	DIP	2.4	CIR

Note. Interplanetary structures associated with each GCR flux <2 day variation are indicated (CIR: corotating interaction region; CHSS: corotating high-speed solar wind streams; HCSC: heliospheric current sheet crossing; MFE: magnetic field enhancement in the slow solar wind; MB: low-energy cosmic rays confined in regions of high magnetic field between two subsequent CHSSs). IMF, solar wind plasma data and near-Earth ICME passages were gathered from https://cdaweb.sci.gsfc.nasa.gov/index.html and http://www.srl.caltech.edu/ACE/ASC/DATA/level3/icmetable2.htm. HCSC are reported in http://omniweb.sci.gsfc.nasa.gov./html/polarity/polarity_tab.html.

out to investigate the characteristics and the origin of these variations. GCR flux depressions and peaks of duration longer than 0.75 days (18 hr) with intensities >2% were studied. GCR flux variations larger than 2% in intensity were considered in order to set the statistical significance of the selection criterion to 2σ, given the 1% the statistical uncertainty on PD hourly averaged single count data. The *LPF* PD observations during each BR were compared to the IMF intensity, solar wind plasma parameters, and NM measurements. Twenty-three, non-recurrent <2 day duration GCR flux variations were observed between 2016 February 18 and 2017 July 3. These 23 variations consisted of 6 enhancements and 17 depressions. As an example, in Figure 11 data gathered during the BR 2492 present a small depression on 2016 April 7–8 and two small peaks on 2016 April 15 and April 23. A comparison of the *LPF* data with those gathered with polar NMs during the same BR 2492 in Figure 13 shows that the small GCR flux enhancement dated April 15 was observed in the most of the polar NM measurements; similarly the depression dated April 7–8 is observed by the Thule and McMurdo NMs. Conversely the April 23 enhancement is not observed in polar NMs. Interplanetary plasma (solar wind bulk speed, temperature, and proton density) and magnetic field parameters are studied to identify interplanetary structures associated with individual <2 day GCR flux variations. In Table 4 CHSSs observed during subsequent BRs and originating from coronal holes are characterized by a solar wind speed >400 km s^{-1}, low magnetic field, and plasma densities. Corotating interaction regions (CIRs) are identified as regions of compressed plasma formed between the leading edges of CHSSs at the interface that separates slow- and fast-stream plasma. Magnetic barriers (MBs) indicate those regions of high plasma magnetic field intensity observed between closely spaced CHSSs. MFE remains for magnetic field enhancements in the slow solar wind. The majority of small depressions in the GCR flux are caused by HCSC; only seldom were their evolutions modulated by CHSS and CIR. These findings were different from those obtained with an analog study carried out in Armano et al. (2018a) for GCR flux-recurrent depressions >2 days, indicating that, in general, these depressions are associated with CIR and with the passage of CHSS. Peaks with duration <2 days appear to be associated with regions of compressed plasma between two CHSS (see, for instance, 2016 April 23–24 in Figure 12). Several processes may generate these small peaks in the GCR flux. The most plausible is that the lowest-energy GCRs (≃70 MeV) are excluded from regions of enhanced IMF intensity between subsequent CHSSs. However, a change in the low-energy GCR spectrum slope between a flux recovery phase after a CHSS passage and a new GCR flux decrease due to the passage of a subsequent CHSS, may also generate a peak feature in the integral flux. An increase of the GCR flux due to the acceleration at the shock of incoming CHSS does not appear plausible on the basis of the absence of small peak structures at the passage of isolated CHSS (see Figure 6 in Armano et al. 2018a). As a matter of fact, both models and observations indicate that the maximum energy of particles accelerated at CIR regions is about 20 MeV (Mc Donald et al. 1975; Bones & Simpson 1976; Tsurutani et al. 1985; Desai et al. 1998; Giacalone et al. 2002; Richardson 2004; Laurenza et al. 2015).

7. Conclusions

A PD on board *LPF* allowed for the measurement of the integral flux variation of GCR protons and helium nuclei above 70 MeV n^{-1}. The energy dependence of the FDs measured on board *LPF* was compared to that of other space experiments and NMs, which allows for direct measurements of the integral flux variation of GCRs above effective energies >10 GeV. A parameterization of pre-decrease energy spectra and energy spectra measured during the main phase of FDs is found to apply to different intensity events.

FDs observed in L1 are not correlated with geomagnetic storm occurrence unless the southward component (B_z) of the IMF presents values <−20 nT. Finally, hourly averaged GCR flux variations measured with *LPF* allowed for the observations of non-recurrent features in the GCR integral flux variations >0.75 days and <2 days with intensities >2%. These short-term depressions and peaks in the data trend appear to be correlated in the majority of cases with HCSC and plasma compression regions between subsequent CHSSs, respectively.

This work is dedicated to the loving memory of Prof. Karel Kudela, a marvelous colleague and a special friend that left us too soon on 2019 January 20.

The authors are grateful to the anonymous referee for the precious comments and suggestions that allowed for a major improvement of the manuscript.

Solar modulation parameter data were gathered from http://cosmicrays.oulu.fi/phi/Phi_mon.txt. Data from the *ACE* experiment were obtained from the NASA-CDAWeb website. We acknowledge the NMDB database (www.nmdb.eu) funded under the European Union's FP7 programme (contract no. 213007), and the PIs of individual NM stations for providing data. HCS crossing was taken from http://omniweb.sci.gsfc.nasa.gov./html/polarity/polarity_tab.html.

This work has been made possible by the *LISA Pathfinder* mission, which is part of the space-science program of the European Space Agency. The French contribution has been supported by the CNES (Accord Specific de projet CNES 1316634/CNRS 103747), the CNRS, the Observatoire de Paris, and the University Paris-Diderot. E. P. and H. I. also acknowledge the financial support of the UnivEarthS Labex program at Sorbonne Paris Cité (ANR-10-LABX-0023 and ANR-11-IDEX-0005-02). The Albert-Einstein-Institut acknowledges the support of the German Space Agency, DLR. The work is supported by the Federal Ministry for Economic Affairs and Energy based on a resolution of the German Bundestag (FKZ 50OQ0501 and FKZ 50OQ1601). The Italian contribution was supported by Agenzia Spaziale Italiana and Instituto Nazionale di Fisica Nucleare. The Spanish contribution was supported by Contracts No. AYA2010-15709 (MICINN), No. ESP2013-47637-P, and No. ESP2015-67234-P (MINECO). M. N. acknowledges support from Fundacion General CSIC (Programa'ComFuturo). F.R. acknowledges an FPI contract (MINECO). The Swiss contribution acknowledges the support of the Swiss Space Office (SSO) via the PRODEX Program of ESA. L. F. acknowledges the support of the Swiss National Science Foundation. The United Kingdom groups acknowledge support from the United Kingdom Space Agency (UKSA), the University of Glasgow, the University of Birmingham, Imperial College, and the Scottish Universities Physics Alliance (SUPA). J. I. T. and J. S. acknowledge the support of the U.S. National Aeronautics and Space Administration (NASA). N. Korsakova acknowledges the support of the Newton International Fellowship from the Royal Society. K.K. was formerly supported by the project CRREAT (reg. CZ.02.1.01/0.0/0.0/15003/0000481) call number 02 15 003 of the Operational Programme Research, Development and Education.

ORCID iDs

N. Finetti https://orcid.org/0000-0002-2004-8955
C. Grimani https://orcid.org/0000-0002-5467-6386
M. Laurenza https://orcid.org/0000-0001-5481-4534
C. F. Sopuerta https://orcid.org/0000-0002-1779-4447

References

Adriani, O., Barbarino, G., Bazilevskaya, G. A., et al. 2011, ApJ, 742, 102
Aguilar, M., Alcaraz, J., Allaby, J., et al. 2002, PhR, 366, 331
Amaro-Seoane, P., Audley, H., Babak, S., et al. 2017, arXiv:1702.00786
Antonucci, F., Armano, M., Audley, H., et al. 2011, CQGra, 28, 094001
Antonucci, F., Armano, M., Audley, H., et al. 2012, CQGra, 29, 124014
Araújo, H. M., Wass, P., Shaul, D., Rochester, G., & Sumner, T. J. 2005, APh, 22, 451
Armano, M., Audley, H., Auger, G., et al. 2016, PhRvL, 116, 231101
Armano, M., Audley, H., Auger, G., et al. 2017, PhRvL, 118, 171101
Armano, M., Audley, H., Baird, J., et al. 2018a, ApJ, 854, 113
Armano, M., Audley, H., Baird, J., et al. 2018b, PhRvL, 120, 061101
Armano, M., Audley, H., Baird, J., et al. 2018c, APh, 98, 28
Armano, M., Audley, H., Baird, J., et al. 2018d, PhRvD, 98, 062001
Badruddin, & Kumar, A. 2015, SoPh, 290, 1271
Barouch, E., & Burlaga, F. 1975, JGR, 80, 449
Beer, J. 2000, in Cosmic Rays and Earth, Space Science Review, ed. J. W. Bieber et al. (Amsterdam: Elsevier), 93
Benella, S., Grimani, C., Laurenza, M., & Consolini, G. 2019, NCimC, in press
Bones, C. W., & Simpson, J. A. 1976, ApJL, 210, L91
Burger, R. A., Potgieter, M. S., & Heber, B. 2000, JGR, 105, 27447
Cane, H. V. 2000, SSRv, 93, 55
Cane, H. V., Richardson, I. G., & von Rosenvinge, T. T. 1996, JGR, 101, 21561
Cañizares, P., Chmeissani, M., Conchillo, A., et al. 2011, CQGra, 28, 094004
Chauhan, M. L., Manjula, J., & Shrivastava, S. K. 2011, ICRC (Beijing), 32, 261
Desai, M. I., Marsden, R. G., Sanderson, T. R., et al. 1998, JGRA, 103, 2003
Dremukhina, L. A., Levitin, A. E., Rudneva, N. M., & Gromova, L. I. 2011, in Physics of Auroral Phenomena, Proc. XXXIII Ann. Seminar, 55, http://pgia.ru:81/seminar/archive/2010/2_fields/02-01_Dremukhina.pdf
Forbush, S. E. 1937, PhRv, 51, 1108
Forbush, S. E. 1954, JGR, 59, 525
Forbush, S. E. 1958, JGR, 63, 651
Giacalone, J., Jokipii, J. R., & Kóta, J. 2002, ApJ, 573, 845
Gil, A., Asvestari, E., Kovaltsov, G. A., & Usoskin, I. 2017, Proc. ICRC (Busan), 35, 032, https://pos.sissa.it/301/032/pdf
Gleeson, L. J., & Axford, W. I. 1968, ApJ, 154, 1011
Gonzales, W. D., Jocelyn, J. A., Kamide, Y., et al. 1994, JGR, 99, 5771
Grimani, C., Araújo, H. M., Fabi, M., et al. 2011, CQGra, 28, 094005
Grimani, C., Benella, S., Fabi, M., Finetti, N., & Telloni, D. 2017, JPhCS, 840, 012037
Grimani, C., Fabi, M., Lobo, A., Mateos, I., & Telloni, D. 2015, CQGra, 32, 035001
Grimani, C., Vocca, H., Bagni, G., et al. 2005, CQGra, 22, S327
Hofer, M. Y., & Flückiger, E. O. 2000, JGR, 105, 23
Kane, R. P. 2010, AnGeo, 28, 479
Kim, R. S., Moon, Y.-J., Gopalswamy, N., Park, Y.-D., & Kim, Y.-H. 2014, SpWea, 12, 246
Laurenza, M., Consolini, G., Storini, M., & Damiani, A. 2015, JPhCS, 632, 012066
Laurenza, M., Vecchio, A., Storini, M., & Carbone, V. 2014, ApJ, 781, 71
Lockwood, J. A. 1971, SSRv, 12, 658
Mateos, I., Diaz-Aguiló, M., Gibert, F., et al. 2012, JPhCS, 363, 012050
McDonald, F. B., Teegarden, B. J., Trainor, J. H., von Rosenvinge, T. T., & Webber, W. R. 1975, ApJL, 203, L149
Munini, R., Boezio, M., Bruno, A., et al. 2018, ApJ, 853, 76
Papini, P., Grimani, C., & Stephens, A. S. 1996, NCimC, 19, 367
Potgieter, M. S. 2013, LRSP, 10, 3
Richardson, I. G. 2004, SSRv, 111, 267

Richardson, I. G., Wibberenz, G., & Cane, H. V. 1996, JGR, 101, 13483
Sabbah, I. 2000, GeoRL, 27, 1823
Sabbah, I. 2007, SoPh, 245, 207
Sabbah, I., & Kudela, K. 2011, JGR, 116, A04103
Shaul, D. N. A., Aplin, K. L., Araújo, H., et al. 2006, in AIP Conf. Proc. 873, Laser Interferometer Space Antenna, ed. S. M. Merkovitz & J. C. Livas (Melville, NY: AIP), 172
Shikaze, Y., Haino, S., Abe, K., et al. 2007, APh, 28, 154
Stone, E. C., Frandsen, A. M., Mewaldt, R. A., et al. 1998, SSRv, 86, 1
Tsurutani, B. T., Burton, M. E., Smith, E. J., & Jones, D. E. 1985, Planet. Space Sci., 35, 289
Usoskin, I. G., Bazilevskaya, G., & Kovaltsov, G. A. 2011, JGR, 116, A02104
Usoskin, I. G., Bazilevskaya, G. A., & Kovaltsov, G. A. 2017, JGRA, 122, 3875
Usoskin, I. G., Braun, I., Gladysheva, O. G., et al. 2008, JGR, 113, A07102
Usoskin, I. G., Kovaltsov, G. A., Adriani, O., et al. 2015, AdSpR, 55, 2940
Wass, P. J., Araújo, H. M., Shaul, D. N. A., & Sumner, T. J. 2005, CQGra, 22, S311